Chapter 8

Atmospheric Absorption

Michel Guélin

IRAM, 300 rue de la Piscine, F-38406 Saint Martin d'Hères

8.1 The Atmosphere

8.1.1 Constituents of the atmosphere

It is convenient to subdivide the atmosphere into a "clean dry" component, water vapor, and aerosols (water droplets, as well as ice crystals, salt grains & dust particles, which serve as condensation seeds for water).

Abundances Table 8.1 gives the composition of the "clean dry" air in the "standard US" model throughout the troposphere (i.e at altitudes $\leq$ 20 km). Altogether, N_2, O_2, and Ar represent 99.96 % in volume. Except for CO_2, whose abundance at ground level may vary between day and night by up to a factor of 2, this composition is remarkably homogeneous and constant. It is completed by a number of trace components, most of which are unstable (SO_2, O_3, NO, CO, ...) and whose abundance (in volume) never exceeds 10^{-5}.

The abundance of water is highly variable, but hardly exceed 1% in mass, even locally. Most of the water in the air is in the form of vapor. Even inside the clouds, precipitation and turbulence insure that

Name	Molec. mass amu	Normal abund. (% in volume)	Name	Molec. mass amu	Normal abund. (% in volume)
N_2	28.013	78.084	He	4.003	0.0005
O_2	32.000	20.946	Kr	83.8	0.0001
Ar	39.948	0.934	CH_4	16.043	0.0002
CO_2	44.010	0.033^v	H_2	2.016	0.00005
Ne	20.183	0.0018	N_2O	44.013	0.00005

Table 8.1: Main constituents of the dry air in the troposphere

the mass of water droplets per cm^{-3} seldom equals that of water vapor.

Despite their low abundances, water, which has a large absorption cross section in the IR and a large specific heat of vaporization, ($L_w \sim 600$ cal/g), ozone and carbon dioxyde, which have large IR absorption cross sections, are the major actors of the thermal balance of the air.

Absorption spectrum Ozone is responsible for most of the absorption of the solar radiation in the UV (especially between 1800 and 2900 Å). In the visible, the air is fairly transparent except for scattering by aerosols (mostly water droplets and/or ice crystals when there are clouds). In the infrared, H_2O, CO_2 and, around 10μm, O_3 are very efficient absorbers of the solar and ground radiation.

By clear weather, the atmospheric absorption at mm wavelengths is dominated by rotational and fine structure lines of molecules in their ground electronic and vibrational state. The strongest transitions are electric dipole transitions from polar molecules, like water and ozone. Intrinsically weaker (typically by a factor of 10^{2-3}), but of considerable practical importance, are the magnetic dipole transitions from O_2. When there are clouds, the thin water droplets scatter and absorb the short (mm) radio waves.

8.1.2 Thermodynamics of the air

Ideal gas For one molecule with n degrees of freedom (e.g. in the rigid-molecule approximation, n= 2 (deg. of rotation) +3 (of transl.) = 5 for O_2 and N_2, and n= 3 + 3 = 6 for H_2O), the internal energy per molecule is

$$U = \mathrm{n} \times \frac{1}{2} kT$$

and for $\mathcal{N}$ molecules of O_2 or N_2,

$$U = \frac{5}{2}\mathcal{N}kT = \frac{5}{2}nRT$$

where n is the number of moles and R the gas constant.

The Enthalpy is

$$H = U + pV = U + \mathcal{N}kT$$

$$c_v = \frac{dU}{dT} = \frac{5}{2}\mathcal{N}k\ , \quad c_p = \frac{dH}{dT} = \frac{7}{2}\mathcal{N}k,\ , \quad \gamma = \frac{c_p}{c_v} = \frac{7}{5} = 1.4$$

For adiabatic expansion, we have the standard relations

$$c_p \mathrm{Log}(\frac{T}{T_0}) - R\mathrm{Log}(\frac{p}{p_0}) = 0 \quad \text{and} \quad T = Cst \times p^m$$

where $m = \frac{R}{c_p} = \frac{\gamma - 1}{\gamma}$ is the Poisson constant.

Gas mixture: Dalton's law A mixture of ideal gases *i= 1, 2, ...* in a volume V behaves like an ideal gas:

$$\text{Partial pressures}: \quad p_1 V = \mathcal{N}_1 kT, \quad p_2 V = \mathcal{N}_2 kT, \quad ... \tag{8.1}$$

$$\text{Total pressure}: \quad pV = (p_1 + p_2)V = (\mathcal{N}_1 + \mathcal{N}_2)kT + ... \quad = \mathcal{N}kT \tag{8.2}$$

Dry air is a mixture of N_2, O_2, ... molecules. It behaves indeed very much like an ideal gas: $R_a = c_{p_a} - c_{v_a} = 8.3143$ J/mol-deg (vs 8.3149 for an ideal gas), γ_a= 1.404 (vs 1.400 for ideal rigid molecules).

Wet air (without clouds) is a mixture of dry air + H_2O molecules. It is customary to denote by e the partial pressure of water vapor, p_a that of dry air, and p' the wet air pressure. The specific heats of water *vapor* are not that different from those of ideal gases: $c_{v_w} = 25.3 + 210^{-3}(T - 273)$; $\gamma_w = 1.37$, vs $c_v = 3R = 24.9$ and $\gamma = \frac{4}{3}$ for a rigid asymmetric top.

Then, Dalton's law yields:

$$c'_v = (1 - \frac{e}{p'})c_{v_a} + \frac{e}{p'}c_{v_w} \simeq (1 + 0.2\frac{e}{p'})c_{v_a} \tag{8.3}$$

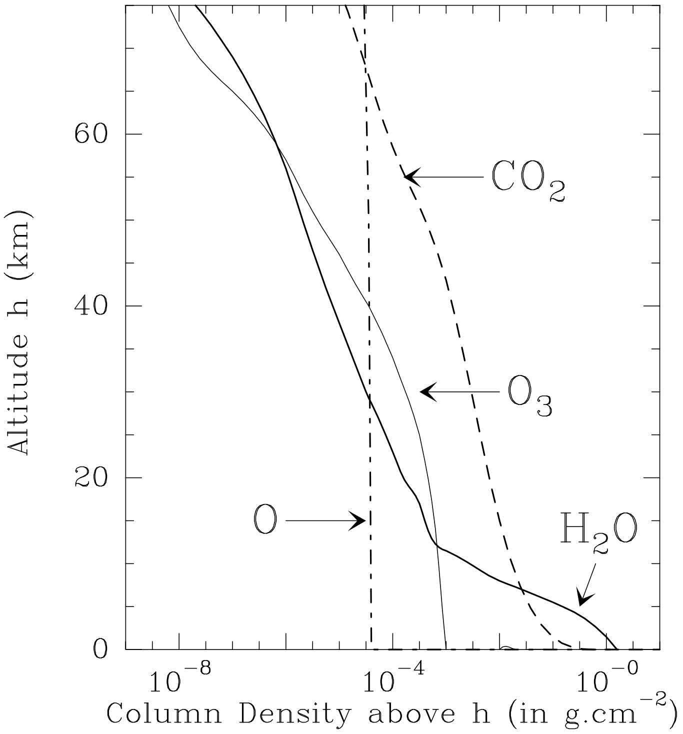

Figure 8.1: Column densities of important atmosphere components above a given altitude – after Queney (1974)

The fractional abundance of water vapor and $\frac{e}{p}$ reaching seldom a few percent, the wet air constants are within a small correction term equal to the dry air constants. In particular, introducing the volume density ρ, it is customary to write:

$$p' = \frac{R\rho' T}{M'} = \frac{R\rho T'}{M_a} \tag{8.4}$$

where $T' = \frac{M'T}{M_a} = T(1 - 0.378\frac{e}{p'})^{-1}$, is the *virtual temperature.*

Then, for the adiabatic expansion of a wet air bubble, one has:

$$T' = Cst \times p^{m'} \tag{8.5}$$

m' is equal to m_a within few per mil, so, in practice, the adiabatic curves of dry air can be used for wet air (without clouds), provided one replaces T by T' (the difference could reach a few K and could be important near 0°C). In the following, we drop the 'prime' signs, except for the virtual temperature T'.

8.1.3 Hydrostatic equilibrium

At large scales, the air pressure and density depend essentially on the massive and slowly varying dry component and are well described by *hydrostatic equilibrium.* The air temperature, as we have seen, depends significantly on the abundance and distribution of water, CO_2 (and O_3 for the stratosphere).

At equilibrium:

$$dp/dh = -g\rho \tag{8.6}$$

$$p = \frac{\rho R T'}{M_a} \tag{8.7}$$

where ρ is the density at an altitude h, p is the pressure, $T' \simeq T$ the air "virtual" temperature. $M_a \simeq 29$ is the average molecular weight, and g the local gravitational field.

$$\frac{dp}{p} = \frac{-gM_a}{RT'}dh \tag{8.8}$$

In the "standard atmosphere" model, T', the temperature of the air varies linearly with altitude and is given throughout the troposphere (i.e. between h=0 and 11 km) by:

$$T' = T'_o - b(h - h_o) \tag{8.9}$$

where $b = 6.5$ K km^{-1} is a constant.

Let us first consider a relatively small change in altitude: $h - h_o \leq 1$ km, $T' \simeq T'_{ave} = (T'(h) + T'(h_o))/2$; we find Laplace's hydrostatic formula:

$$\frac{\rho}{\rho_0} \simeq \frac{p}{p_0} \simeq e^{-\frac{gM_a h}{RT'_{ave}}} = e^{-\frac{h}{h_o}} \tag{8.10}$$

where ρ_o is the density at sea level and $h_o = RT/M_a g = 8.4(T/288)$ km, the scale height. The gas column density (expressed in g.cm^{-2}) along the vertical above a point at sea level is:

$$N_o M_a = \int \rho dh = \rho_o h_o \tag{8.11}$$

and that above a point at an altitude h:

$$N = N_o e^{-h/h_o} \tag{8.12}$$

For larger altitudes, from Eq.8.8 $dh = -dT'/b$, then Eq.8.9 yields

$$\frac{dp}{p} = \frac{-gM_a dh}{bR}\frac{dT'}{T'} \tag{8.13}$$

$$\rho = \rho_o(\frac{T'}{T'_o})^{s-1} \tag{8.14}$$

with $s = -g/(bR_a)$.

Although the above equations represent fairly well the density and pressure throughout the troposphere, the temperature distribution can depart significantly from Eq.8.9 near the ground. This latter heats up faster than the transparent air during the day, and cools off more rapidly during the night. The temperature gradient at low altitudes (up to 1-2 km) can be thus steeper or shallower than shown in Eq.8.9. Occasionally, it can be inverted, the temperature increasing with altitude. The *inversion layer* usually stops briskly at 1 or 2 km altitude and the normal temperature gradient resumes above. Inversion layers are common during the night over bare land. They can also be caused by hot winds blowing from the sea.

The local temperature gradient determines stability of the air to vertical motions. A rising bubble of wet air expands adiabatically as long as the water vapor it contains does not condense. Expanding, it cools almost as an ideal gas with:

$$T \propto p^m \text{ and } m = (1 - 0.23q)m_a \simeq m_a \tag{8.15}$$

The pressure is set by the surrounding air (Eq.8.10), and the bubble seen to cool down with an "adiabatic" gradient of

$$\frac{dT}{dh} = -g\frac{M_a}{C_p} = 9.8\text{Kkm}^{-1}$$

If the actual temperature gradient is smaller than the adiabatic gradient, the bubble becomes cooler, hence denser than the surrounding air and its ascent stops. The air is stable. If the local gradient is larger than the adiabatic gradient, the bubble becomes less dense than the surrounding air; the air is unstable and a thick convection layer develops, a situation likely to happen in a hot summer afternoon.

8.1.4 Water

The scale height of water, h_w, which results from a fast evaporation/condensation process, is small (typically 2 km) compared to the equilibrium scale height $h_o = 8.4$ km. At $h = 2.5$ km, the altitude of the Plateau de Bure, the water vapor column density N_w (or w, "amount of precipitable water", when expressed in g.cm^{-2}, or cm of water) is normally reduced by a factor of 3-4, with respect to sea level. This factor, as we have seen, is strongly modulated by the local temperature gradient. w is lower in the presence of a low altitude inversion layer which reduces the vertical turbulence and traps most of the water well below the observatory.

The value of w on a site can be estimated directly by measuring the air pressure p_{tot} (in mbar), temperature T (in K) and relative humidity RH (in percent), and using the formulas 8.7 and 8.11 adapted for water (the air pressure p is replaced by the partial water vapor pressure e):

$$w[\text{mm}] = \rho_w[\text{gm}^{-3}]h_w[\text{km}] \tag{8.16}$$

$$\rho_w[\text{gm}^{-3}] = \frac{eM_w}{RT} = 216.5e[\text{mbar}]/T[\text{K}] \tag{8.17}$$

e is related to $e_s(T)$, the water vapor pressure in saturated air, by:

$$e = RH \cdot e_s/100 \tag{8.18}$$

e_s is a rather complex function of T, for which an approximate analytical expression, as well as tabulated values, can be found in the literature (see e.g. [Queney 1974], p.120). To the zero order, it can be expressed by:

$$e_s[mbar] \simeq 6(T/273)^{18} \tag{8.19}$$

8.1.5 Photodissociation products

Ozone is formed from the reaction of O_2 with atomic oxygen, the latter resulting from the photodissociation of O_2 in the upper atmosphere. Ozone is inexistent below 10 km; its opacity becomes comparable to that of H_2O above 15 km where its relative abundance may reach 10^{-5} (see Fig.8.1). At short millimeter wavelengths, it causes narrow absorption lines (mostly above 230 GHz).

The other trace atmospheric components CH_4, SO_2, CO, N_2O, NO, etc.. have very low abundance and, even polar, play no significant role, their maximum opacities being typically more than 10 times smaller than those of ozone.

8.2 Spectroscopy of H_2O, O_2, O_3

Of the major molecular constituents of the atmosphere (see Table 8.1 and Fig. 8.1), only water vapor and ozone, owing to their bent structure, have a non-zero electric dipole moment. Molecular nitrogen, an homonuclear species, and CO_2, a linear symmetric species, have no permanent electric or magnetic dipole moment in their lowest energy states. These latter molecules, as is the case for 99.9% of gaseous molecules, are singlet states, with electrons arranged two-by-two with opposite spins.

8.2.1 Water vapor

The rotational energy level diagram of water is shown on Fig.8.2. Each level is denoted, as usual for asymmetric top molecules, by three numbers $J_{K_{-1},K_{+1}}$. J, which is a "good" quantum number, represents the total angular momentum of the molecule; by analogy with symmetric tops, K_{-1} and K_{+1} stand for the rotational angular momenta around the axis of least and greatest inertia. Allowed radiative transitions obey the selection rules $\Delta J = \pm 1, \Delta K = \pm 1, 3$, with K_{-1}, K_{+1} : $odd, odd \leftrightarrow even, even$ or $o, e \leftrightarrow e, o$. The levels with K_{-1} and K_{+1} of the same parity are called *para* levels, those of opposite parity, *ortho* levels. Transitions between ortho and para levels are forbidden; due to the presence of two symmetrical hydrogen

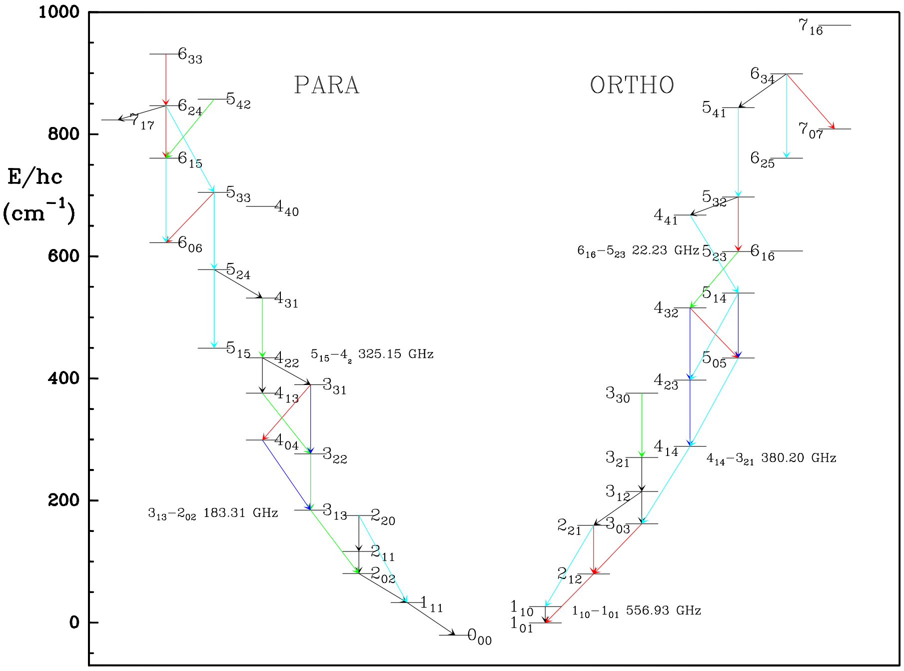

Figure 8.2: The rotational energy level diagram of water vapor

nuclei, the ortho levels have a nuclear statistical weight 3 times larger than the para levels of same J (see e.g. [Townes & Schawlow 1975]). The arrows in Fig.8.2 show the transitions which will be observed by the satellite FIRST (J.Cernicharo, private communication).

8.2.2 Molecular oxygen

Molecular oxygen, although homonuclear, hence with zero electric dipole moment, has a triplet electronic ground state, with two electrons paired with parallel spins. The resulting electronic spin couples efficiently with the magnetic fields caused by the end-over-end rotation of the molecule, yielding a "large" magnetic dipole moment, $\mu^{mag} = 10^{-20}$ emu. The magnetic dipole transitions of O_2 have intrinsic strengths $\sim 10^{2-3}$ times weaker than the water transitions. O_2, however, is 10^{2-3} times more abundant than H_2O, so that the atmospheric lines of the two species have comparable intensities.

The spin of 1 makes of the ground electronic state of O_2 a triplet state ($^3\Sigma$). $\mathbf{N}$, the rotational angular momentum couples with $\mathbf{S}$, the electronic spin, to give $\mathbf{J}$ the total angular momentum: $\mathbf{N} + \mathbf{S} = \mathbf{J}$. The $\mathbf{N}{\cdot}\mathbf{S}$ interaction (and the electronic angular momentum–electronic spin interaction $\mathbf{L}{\cdot}\mathbf{S}$) split each rotational level of rotational quantum number $N \geq 1$ into three sublevels with total quantum numbers

$$J = N + 1, J = N \quad \text{and} \quad J = N - 1$$

the $J = N + 1$ and $J = N - 1$ sublevels lying below the $J = N$ sublevel by approximately $119(N + 1)/(2N + 3)$ GHz and $119/(2N - 1)$ GHz, respectively ([Townes & Schawlow 1975] p.182). Note that the two identical ^{16}O nuclei have spins equal to zero and obey the Bose-Einstein statistics; there are only odd N rotational levels in such a molecule.

The magnetic dipole transitions obey the rules $\Delta N = 0, \pm 2$ and $\Delta J = 0, \pm 1$. Transitions within the fine structure sublevels of a rotational level (i.e. $\Delta N = 0$) are thus allowed. The first such transition is the $(J, N) = 1, 1 \leftarrow 0, 1$ transition, which has a frequency of 118.75 GHz. The second, the $1, 1 \leftarrow 2, 1$ transition, has a frequency of 56.26 GHz. It is surrounded by a forest of other fine structure transitions with frequencies ranging from 53 GHz to 66 GHz. The first "true" rotational transition, the $N = 3 \leftarrow 1$ transitions, have frequencies above 368 GHz (368.5, 424.8, and 487.3 GHz).

The rare isotopomer $^{18}O^{16}O$ is not homonuclear, hence has odd N levels and a non-zero electric dipole moment. This latter, however, is vanishingly small (10^{-5}D). $^{18}O^{16}O$, moreover, has a very low abundance

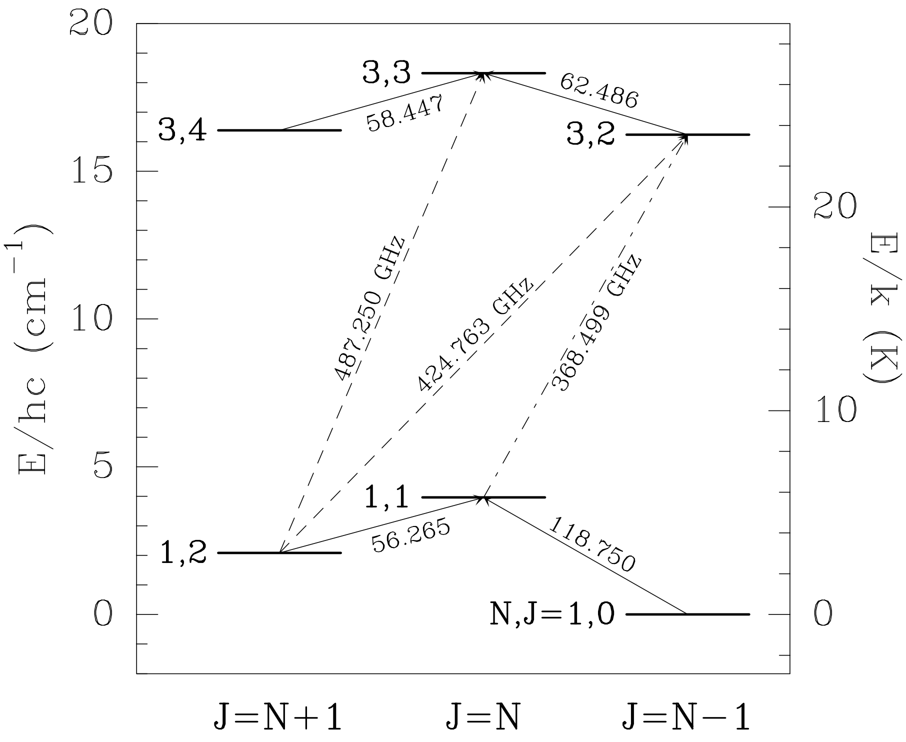

Figure 8.3: The rotational energy level diagram of molecular oxygen

(few hundred times smaller than the main isotopomer), so that its magnetic dipole transitions (even the $\Delta N = 2$, which have stronger intrinsic strengths), can be neglected.

The line opacity and absorption coefficients of $^{16}O_2$ are given by relations similar to Eq.8.24 and Eq.8.25.

8.2.3 Ozone

As noted above, ozone is mostly concentrated between 11 and 40 km altitude; it shows large seasonal and, mostly, latitude variation. Because of its high altitude location, its lines are narrow: at 25 km, ρ_a, hence $\Delta\nu$, is reduced by a factor of 20 with respect to see level; moreover, the dipole moment of ozone (μ= 0.53 D), 3.5 times smaller than that of H_2O, further reduces the ozone line widths.

Because of their small widths and despite the small ozone abundance, ozone lines have significant peak opacities, especially above 230 GHz ($\tau_o = 0.2 - 0.3$).

8.3 Propagation of a wave in the atmosphere – Line shapes

A plane wave propagating along the z direction in the atmosphere can be represented by its electric field vector **E**:

$$\mathbf{E}(z,t) = \mathbf{E}_m e^{-j2\pi\nu(t - n_c \frac{z}{c})} \tag{8.20}$$

where $n_c = n + jn_i$ is the complex refraction index.

The real part, the true refraction index, $n = c/v_p$ (where v_p is the phase velocity of the wave), is often expressed in terms of the refractivity,

$$N = 10^6(n-1) \simeq 0.223\rho_a + 1760\rho_w/T \tag{8.21}$$

The right hand sum, which was empirically derived, is known as the Smith-Weintraub equation. It separates the contribution of the dry air component (first term, where ρ_a is the air density, expressed in gm^{-3}) from that of water vapor (second term, where ρ_w is the density of water vapor).

The imaginary part of the refraction index, n_j causes an exponential attenuation of the wave amplitude, and is related to the power absorption coefficient κ_ν by:

$$n_j = \frac{c\kappa_\nu}{4\pi\nu} \tag{8.22}$$

At a frequency ν close to a rotational transition $\nu_{lu} = (E_u - E_l)/h$, the optical depth is:

$$\tau_\nu = \int \kappa_\nu(T, P)dh \tag{8.23}$$

κ_{lu}, the absorption coefficient integrated over the transition lu is given by the standard asymmetric top formula (see e.g. [Townes & Schawlow 1975] p.102):

$$\kappa_{lu} = \frac{8\pi^2 h^{1.5}}{3c(kT)^{2.5}}(\frac{\rho_w}{m_w})g_I\sqrt{ABC}\mu^2 S_{lu}T^{-2.5}(1-\frac{h\nu}{kT})e^{E_l/kT}\nu_{lu}^2\Phi(\nu-\nu_o) \tag{8.24}$$

Replacing A, B, C, the rotational constants (here in Hz), and μ = 1.85 Debye = $1.85\,10^{-18}$ esu.cm, the electric dipole moment, by their values for H_2O, and setting $(1 - \frac{h\nu}{kT}) = 1$,

$$\kappa_{lu}^w[cm^{-1}] = 5.710^{-24}(\rho_w/m_w)g_I S_{lu}(T/273)^{-2.5}e^{E_l/kT}\nu_{lu}^2\Phi(\nu-\nu_o) \tag{8.25}$$

S_{lu} is the transition intrinsic strength, g_I= 3/2 or 1/2 is the nuclear relative statistical weight of the ortho and para levels (see below), and $\Phi(\nu - \nu_o)$ the line profile. ν_{lu} is now in GHz.

The line profile is given to a good approximation by the well known Van Vleck and Weisskopf collisional profile (here, multiplied by π, [Townes & Schawlow 1975] p.342):

$$\Phi(\nu-\nu_o) = \frac{\Delta\nu}{(\nu-\nu_o)^2 + (\Delta\nu)^2} + \frac{\Delta\nu}{(\nu+\nu_o)^2 + (\Delta\nu)^2} \tag{8.26}$$

with $\Delta\nu = \frac{1}{2\pi\tau}$, where $\Delta\nu$ is the line width and τ the mean time between molecular collisions.

At the centre of the line, the second term of Eq.8.26 becomes negligible, and

$$\Phi(\nu-\nu_o) = 1/\Delta\nu = 2\pi\tau \sim \frac{2\pi}{\frac{\rho_a}{m_a}v\sigma^2} \tag{8.27}$$

$v \sim \sqrt{T}$ is the molecular velocity and σ the collisional cross section.

Note that the density in Eq.8.24 is ρ_w, whereas that in Eq.8.27 is ρ_a: the absorption coefficient at the centre of the line is proportional to ρ_w/ρ_a. It is independent of the total air pressure, as long as this ratio (hence RH) stays constant. This is not the case, of course, away from the centre, since $\Delta\nu \sim \rho$: as the density drops, the lines become narrower and narrower. In the far wings of the line, the second term in Eq.8.26 and the contribution from the wings of other lines cannot anymore be neglected. In fact, a better fit to the water emission in the far wings is reached if Eq.8.26 is replaced by another collisional line shape, called the "kinetic profile"

$$\Phi(\nu-\nu_0) = \frac{4\nu\nu_0\Delta\nu}{(\nu^2-\nu_0^2)^2 + 4\nu^2\Delta\nu^2} \tag{8.28}$$

The opacity and width of the main $H_2^{16}O$ lines are large: $\tau_o = 60$ and $\Delta\nu \simeq$ 20GHz, for the fundamental line in normal conditions of p and T, and for ρ_w = 1g.m^{-3} and w_w= 1 mm (dry weather). These lines dominate most of the millimetre and submillimetre atmospheric attenuation; deviations from theoretical line shapes in the far wings (typically 1/10th of intensity) are accounted for by an empirical continuum. The rare isotopomer $H_2^{18}O$, a few hundred times less abundant than $H_2^{16}O$, makes a negligible contribution (see the discussion by [Waters 1976])

8.4 The atmospheric absorption spectrum at millimeter wavelengths, ATM

Calculations of zenith atmosphere opacity at 2.5 and 2.9 km, the altitude of the IRAM sites, have been made by [Cernicharo 1988] and [Cernicharo & Pardo 1999]. A computer programme, ATM, repeating these calculations has been installed on-line on the IRAM telescopes of Pico Veleta and Plateau de Bure; it is activated at each calibration or skydip and allows to interpret the observed sky emissivity in terms of water and oxygen contributions and of upper and lower sideband opacities. (During skydips, the antenna is pointed successively at different elevations and the emission of the sky measured at each step; the sky emission variation is fitted by an exponential function of the air mass, and the atmosphere opacity and average temperature readily derived). Note that the opacities derived from sky emissivity observations do not always agree with those calculated from the measurement of p, T, and RH on the site, as water vapor is not at hydrostatic equilibrium.

Some of the results for the band 20–500 GHz are shown on Fig.8.4. One recognizes from left to right, the (blended) forest of fine structure transitions from O_2, near 60 GHz, the $1,1 \leftarrow 0,1$ fine structure line of O_2 at 118.75 GHz, the third lowest lines of para water (still 200 K above the ground level), at 183.31 GHz, and the fourth ortho water line (420 K above ortho ground level), at 325.15 GHz. The fundamental line of ortho water ($1_{10} \leftarrow 1_{01}$), at 556.94 GHz is visible. The water and oxygen lines delineate the 4 atmospheric "windows" of the millimetre spectrum (called the 3 mm, 2 mm, 1.3 mm and 0.8 mm windows). Water is seen to dominate completely atmospheric absorption above 150 GHz.

Less than one millimeter of precipitable water vapor corresponds to exceptionally good winter weather conditions on the sites of Pico Veleta and Plateau de Bure. Such conditions seldom happen even on Mauna Kea. Two to three millimeter of water are standard by clear winter nights at these observatories; six to ten millimeter of water are typical of clear summer nights.

The typical zenith atmosphere opacities, in the dips of the 1.3 mm and 0.8 mm windows (e.g. at the frequencies of the $J = 2-1$ and $3-2$ rotational transitions of CO, 230.54 and 345.80 GHz), are respectively 0.15–0.2 and 0.5–0.7 in winter. The astronomical signals at these frequencies are attenuated by factors of respectively $\simeq$ 1.2 and 2 at zenith, 1.3 and 2.8 at 45 degree elevation, and 1.7 and 6 at 20 degree elevation. Larger attenuations are the rule in summer and in winter by less favorable conditions.

The $J = 1-0$ line of CO, at 115.27 GHz, is close to the 118.75 GHz oxygen line. Although this latter is relatively narrow, it raises by $\simeq$0.3 the atmosphere opacity (which is 0.35–0.4). The atmosphere attenuation is then intermediate between those at 230 and 345 GHz (by dry weather, however, it is more stable than the latter, since the water contribution is small). The measurement of accurate CO line intensity ratios (even not considering the problems linked to differences in beam size and receiver sideband gain ratios) requires therefore good weather, a high source elevation, and a careful monitoring of the atmosphere.

A catalogue of lines intensities in several standard astronomical sources, measured with the IRAM 30 m telescope has been published [Mauersberger et al 1989]. The lines intensities were calibrated by the chopper-wheel method, following the above recipes. The reader is referred to this report for details.

8.5 Correction for atmospheric absorption, T_A^*

By analogy with the Rayleigh-Jeans approximation, $I = 2kT/\lambda^2$, which strictly applies to long wavelengths, the mm-wave radio astronomers have introduced the concept of "radiation" or "effective" temperatures, which scale *linearly* with the detected power.

The noise power detected by the telescope is the sum of the power received by the antenna, $\mathcal{W}_A$, and of the noise generated by the receiver and transmission lines, $\mathcal{W}_{rec}$.

Using Nyquist's relation $\mathcal{W} = kT\Delta\nu$, $\mathcal{W}_A$ and $\mathcal{W}_{rec}$ can be expressed in terms of the temperatures T_A and T_{rec} of two resistors, located at the end of the transmission line, which would yield noise powers equal to $\mathcal{W}_A$ and $\mathcal{W}_{rec}$, respectively:

$$\mathcal{W}_A + \mathcal{W}_{rec} = kT_A\Delta\nu + kT_{rec}\Delta\nu = k(T_A + T_{rec})\Delta\nu.$$

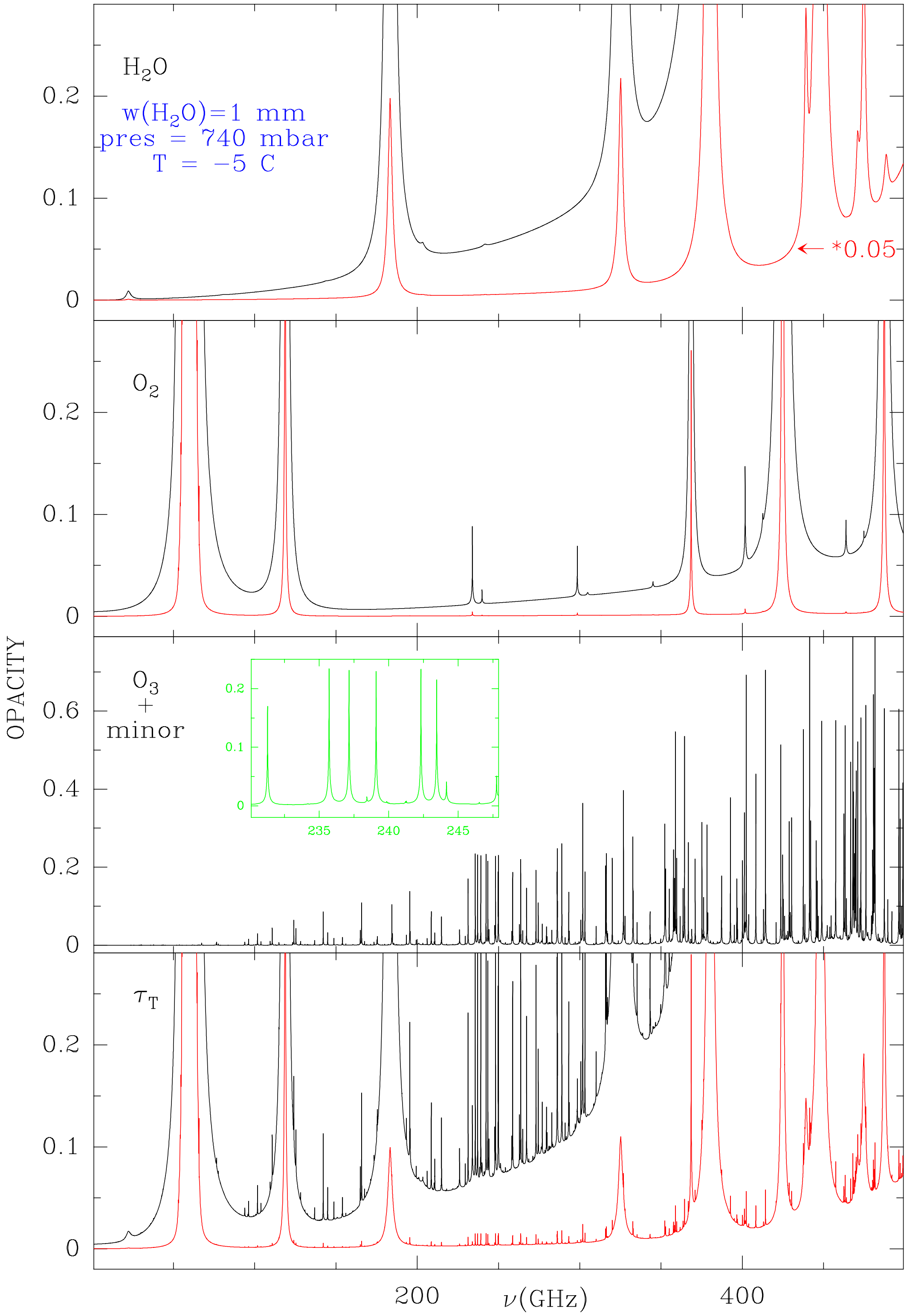

Figure 8.4: Zenith opacity of the standard winter atmosphere at an altitude of 2.5 km for 1 mm of precipitable water vapor, as a function of frequency (GHz). The contributions of H_2O, O_2 and O_3 are shown in the three upper panels. The red line shows the same zenith opacity at a scale of 1/20. One may note the importance of the water line wings above 150 GHz, compared to those of O_2 (a consequence of the absence of electric dipole moment in the latter molecule) and O_3. Courtesy [Cernicharo & Pardo 1999]

T_A is called the "antenna temperature" and T_{rec} the "receiver temperature". T_A becomes T_{load} when the receiver horn sees a load, instead of the antenna, and T_{gr} when it sees the ground. It should be noted that T_{load} and T_{gr} are not stricto sensus equal to the load and ground physical temperatures, but are only "Rayleigh-Jeans" equivalent of these temperatures (they are proportional to the radiated power). For ambient loads, they approach however closely the physical temperature, since $h\nu/k \simeq 11$ K at $\lambda = 1.3$ mm.

When observing with the antenna a source and an adjacent emission-free reference field, one sees a change $\Delta T_A = T_A(sou) - T_A(ref)$ in antenna temperature.

Because of the calibration method explained below, it is customary, in mm-wave astronomy, to replace ΔT_A, the source antenna temperature, by ΔT_A^*, the source antenna temperature corrected for atmosphere absorption and spillover losses. Both are related through:

$$T_A = (1-\eta_f)T_{gr} + \eta_f(T_{sky} + \Delta T_A^* e^{-\tau})$$

where τ is the line-of-sight atmosphere opacity. η_f and η_b are the forward and beam efficiency factors, which denote the fractions of the power radiated by the antenna on the sky and in the main beam, respectively (they are typically of the order of 0.9 and 0.7).

The source equivalent "radiation temperature" T_R (often improperly called "brightness temperature" and therefore denoted T_{MB} when it is averaged over the main beam) and ΔT_A^* are related through

$$\Delta T_A^* = \int_{sou} T_R \mathcal{A}(x,y)dxdy$$

where $\mathcal{A}(x,y)$ is the antenna power pattern. For a source smaller than the main beam, $\Delta T_A* = \eta_b T_{MB}$.

When observing a small astronomical source with an antenna temperature $\Delta T_A' >> T_{BG} = 2.7$ K, located at an elevation el, one detects a signal $\mathcal{V}$ (of scale: $\mathcal{G}$ volt or counts per Kelvin):

$$\frac{\mathcal{V}_{sour}}{\mathcal{G}} = M_{sour} = T_{rec} + (1-\eta_f)T_{gr} + \eta_f T_{sky} + \eta_b \Delta T_A' e^{-\tau} \tag{8.29}$$

This signal can be compared with the signals observed on the blank sky (T_{atm}), close to the source, and to that observed on a hot load (T_{load}):

$$\begin{aligned} M_{atm} &= T_{rec} + (1-\eta_f)T_{gr} + \eta_f T_{sky} \\ T_{sky} &= (1-e^{-\tau})T_{atm} \\ M_{load} &= T_{rec} + T_{load} \end{aligned} \tag{8.30}$$

here, we have neglected the cosmologic background and assume, in a first step, that the receiver is tuned single sideband.

8.5.1 Simplest case

Let's assume that $T_{load} \simeq T_{gr} \simeq T_{atm}$; then:

$$\begin{aligned} M_{load} - M_{atm} &= \eta_f T_{gr} e^{-\tau} \\ M_{sou} - M_{atm} &= \Delta T_A^* e^{-\tau} \\ \Delta T_A^* &= \frac{M_{sou} - M_{atm}}{M_{load} - M_{atm}} \eta_f T_{gr} \end{aligned} \tag{8.31}$$

Note that in Eq.8.31, the measurement of the antenna temperature includes the atmospheric opacity correction, but does not depend explicitly on an assumption on the atmospheric opacity. We can write:

$$\Delta T_A^* = \frac{M_{sou} - M_{atm}}{M_{load} - M_{atm}} \mathbf{T_{cal}} \tag{8.32}$$

where we define T_{cal} as $T_{cal} = \eta_f T_{gr} \simeq \eta_f T_{atm}$.

8.5.2 More realistic case

Typically, the mean atmosphere temperature is lower than the ambient temperature near the ground by about 40 K: $T_{atm} \simeq T_{gr} - 40$ K; then, the formula above still holds *if we replace* T_{cal} by:

$$\begin{aligned} T_{cal} &= (T_{load} - T_{emi})e^{\tau} && (8.33) \\ \text{with } T_{emi} &= T_{sky}\eta_f + (1-\eta_f)T_{gr} \\ &= \frac{(T_{load} + T_{rec}) \times M_{atm}}{M_{load}} - T_{rec} && (8.34) \\ T_{sky} &= (1 - e^{-\tau})(T_{gr} - 40) \end{aligned}$$

T_{rec}, the receiver effective temperature is usually calculated by the Y factor method using a cold load (usually cooled in liquid nitrogen, i.e. at 77 K) and an ambient load (e.g. at 290 K).

$$\begin{aligned} Y &= \frac{M_{hot\_load}}{M_{cold\_load}} \\ T_{rec} &= \frac{T_{hot\_load} - YT_{cold\_load}}{Y-1} && (8.35) \end{aligned}$$

8.5.3 General case

The receiver is not purely single-sideband. Let us denote by G^l and G^u the normalized gains in the receiver lower and upper sidebands, $G^l + G^u = 1$. The atmosphere opacity per km varies with altitude as does the air temperature.

Then, the above expressions of T_{sky} and T_{emi} should be explicited for each sideband ($j = u$ or l):

$$\begin{aligned} T^j_{sky} &= (1 - e^{-\tau^j})T^j_{atm} && (8.36) \\ T_{emi} &= T^l_{sky}\eta_f G^l + T^u_{sky}\eta_f G^u + (1-\eta_f)T_{gr} && (8.37) \end{aligned}$$

The atmospheric transmission model ATM [Cernicharo 1988] allows to calculate iteratively τ_ν from a load+ sky measurement. The values of τ^l, τ^u are calculated for the Standard US atmosphere (parameters are: Winter-, Spring-, or Summer-temperature T, altitude, latitude, water vapor w) by summing up the contributions of O_2 ($A_\nu(T)$), H_2O ($B_\nu(T)$) and O_3 ($C_\nu(T)$) (including rare isotopes and vibrationally excited states):

$$\tau_\nu = A_\nu(T) + wB_\nu(T) + C_\nu(T) \tag{8.38}$$

Depending on ν, the values of $A_\nu(T), B_\nu(T), C_\nu(T)$ are derived either from a Table or estimated from empirical formulae. A first guess of the amount of precipitable water is made from the ambient temperature, pressure and humidity by using the relations of Sec.8.1.4. Then, the expected T_{sky} and T_{emi} are calculated from the two expressions above and T_{emi} is compared to its value measured from the the observation of the atmosphere and the load (Eq.8.35). The value of w is changed and the calculation of τ^j, T^j_{sky} and T_{emi} restarted. Normally, the process converges after 2 to 4 iterations. Once w and T_{emi} are known, the calibration factor T_{cal} can be derived

$$T^j_{cal} = (T_{load} - T_{emi})e^{\tau^j} \tag{8.39}$$

and the data calibrated in the T^*_A scale using Eq.8.32.